3rd International Conference Advanced Mechanics: Structure, Materials, Tribology

Experimental Study of Mesoscale Deformation-Induced Surface Roughening in Commercially Pure Titanium under Low-Cycle Fatigue

AIPCP25-CF-AMSMT2025-00019 | Article

Submitted on: 25-12-2025

Experimental Study of Mesoscale Deformation-Induced Surface Roughening in Commercially Pure Titanium under Low-Cycle Fatigue

Evgeniya Emelianova[1, a)], Maxim Pisarev[1, b)] and Varvara Romanova[1,2, c)]

[1]*Institute of Strength Physics and Materials Science SB RAS, 2/4 pr. Akademicheskii, Tomsk, 634055, Russia*
[2]*National Research Tomsk State University, 36 Lenin ave., Tomsk, 634050, Russia*

[a)] Corresponding author: emelianova@ispms.ru
[b)]pisarev@ispms.ru
[c)]varvara@ispms.ru

Abstract. This paper experimentally investigates mesoscale deformation-induced surface roughening in α-titanium under cyclic loading. Two series of low-cycle fatigue tests are performed under an asymmetric loading-unloading cycle (R=0). In the first series, the stress amplitude remains constant until failure; in the second series, it is gradually increased with the number of cycles. Surface profiles are taken every 10,000 cycles. Displacement and strain fields are monitored in situ using digital image correlation. The deformation-induced surface roughness is quantified using a dimensionless roughness parameter R_d. Surface roughness is observed to appear during the first 10,000 cycles, evolving uniformly across the specimen gauge parts on further loading. The dimensionless roughness parameter does not correlate with the number of cycles under the constant stress amplitude but grows linearly when the peak stress is increased.

INTRODUCTION

Fatigue cracking is a common form of component failure resulting from the gradual accumulation of irreversible deformation and damage at the micro- and mesoscales [1-4]. Generally, the stress level causing fatigue failure is significantly lower than that required to produce fracture under static loading [5, 6]. Therefore, studying the deformation behavior and fracture patterns at micro- and mesoscales and linking them to the macroscopic material response is essential for quantifying the stress-strain state and predicting the onset of failure.

Extensive experimental and numerical studies [see, e.g., 4, 7, 8] demonstrate that valuable information can be obtained from the analysis of deformation-induced surface roughening (DISR). According to Refs. [8, 9], DISR develops hierarchically throughout length scales, including (i) dislocation steps within individual grains at the micoscale, (i) orange peel, ridging, and roping, originating from the relative out-of-plane displacements of individual grains and grain groups at the mesoscale, and (iii) the surface waviness that can be seen by the naked eye at the macroscale. Unlike surface roughness produced by the external actions such as tribological contact [10-13] or thermal exposure [14], the free surface roughening arises from the internal stress-strain state developing in the bulk of the material and, thus, reflects the internal deformation processes.

Our previous investigations [15, 16] have revealed that specific characteristics of mesoscopic DISR correlate with local in-plane plastic strain under uniaxial tension and may serve as early indicators of plastic strain localization and fracture in titanium and aluminum alloys. The numerical study [17] performed for a single loading-unloading cycle demonstrates that plastic deformation begins in individual grains before the macroscopic yield strength is reached, implying that DISR can be expected even at low stresses after a large number of cycles. In this paper, we continue investigations along these lines, analyzing the DISR phenomenon in commercially pure titanium (CP-Ti) under low-cycle fatigue.

EXPERIMENTAL PROCEDURE

For low-cycle fatigue (LCF) tests, the dog-bone-shaped specimens with 36×12×3 mm^3 gauge parts (Fig. 1a) were cut along the axis of a CP-Ti rod (Fig. 1b) in accordance with ASTM E466–15 [18]. Both sides of each specimen were mechanically polished. A speckle pattern was applied to one surface for digital image correlation (DIC) analysis (Fig. 2a), while the opposite surface was divided into 7 equal sections by a set of marks for the surface profile measurements (Fig. 2b).

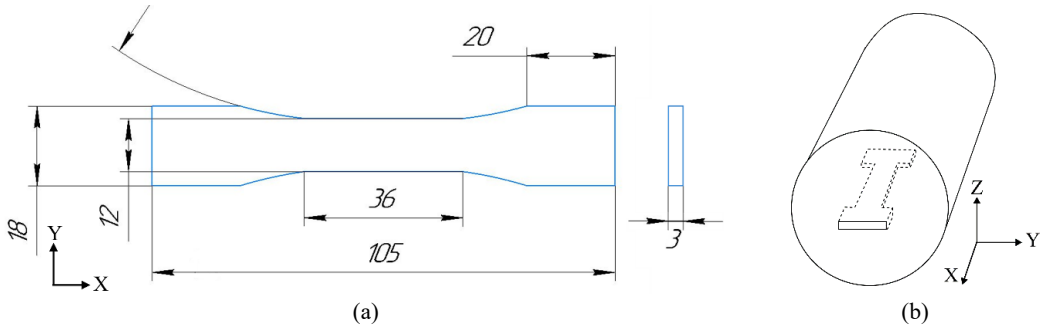

FIGURE 1. Specimen geometry (a) and scheme of cutting out a specimen along the CP-Ti rod axis (b)

FIGURE 2. Specimen surfaces prepared for DIC analysis (a) and contact profilometry (b)

LCF tests were performed on a Biss Nano 15 kN universal testing machine equipped with the Vic-3D DIC system. The tests followed an asymmetrical loading-unloading cycle (stress ratio R=0). The specimens were taken out of the machine every 10,000 cycles to register surface profiles along the specimen central lines. Then, the specimens were put back into the machine and their LCF testing was continued. The process was repeated until failure.

The engineering strains of the specimen sections were calculated as

$$\varepsilon_{loc}=(L_{loc}/L_{loc0})-1, \quad (1)$$

where L_{loc} and L_{loc0} are the current and initial section lengths, respectively, measured as the distance between the marks.

To quantify the evolution of surface asperities, the mesoscopic roughness parameter R_d was calculated for the set of profiles, as proposed in [16]:

$$R_d=L_p/L_b-1, \quad (2)$$

where L_p is the rough profile length and L_b is the profile evaluation length.

Two series of LCF tests were conducted where (1) the stress amplitude remained constant at 315 MPa until failure or (2) was gradually increased from 250 to 315 MPa with the number of cycles. Displacement and strain fields were *in situ* monitored and recorded by the DIC system every 100 cycles at both maximum and minimum stress levels. The selected surface areas were analyzed using the optical profiler NewView 6200.

RESULTS

For both test series, roughening appeared on the specimen free surface already under the first 10,000 loading cycles. All specimens demonstrated qualitatively similar surface morphology characterized by a hierarchical structure. As an illustration, Figure 3 presents the surface profiles obtained after 10,000 and 90,000 loading-unloading cycles under a constant stress amplitude at various magnifications. The black curves represent the measurements taken along the entire gauge length, while the selected fragments magnified by ×10 and ×100 are colored red and blue, respectively. The surface profiles contain periodically repeated peaks and valleys with smaller undulations embedded within the larger-scale ones. The hierarchical structure of the surface features formed after 10,000 cycles remained unchanged on further LCF loading (cf. profiles after 10,000 and 90,000 cycles in Fig. 3). Following the terminology introduced in [19], the surface irregularities observed over 0.4 mm and 4 mm evaluation lengths are hereinafter referred to as meso-I and meso-II.

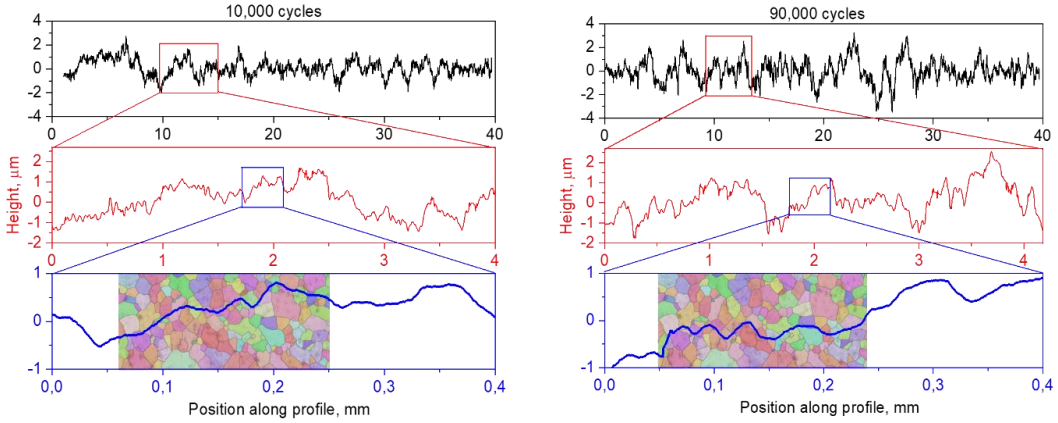

FIGURE 3. Hierarchy of surface irregularities in the profiles measured in a CP-Ti specimen after 10,000 (a) and 90,000 cycles (b) at the constant stress amplitude

Comparing the meso-I surface profiles with the grain structures obtained by electron backscatter diffraction indicates that the finest morphological features resolved within the 0.4 mm evaluation length (blue plots in Fig.3) correspond to the out-of-plane displacements of small grain groups involving up to 5 grains, while larger-sized irregularities are formed by ~20 grains. Even larger surface undulations spanning up to 0.5 mm are resolved after 10,000 cycles within the 4 mm evaluation length at the meso-II scale (red plot in Fig. 3a). After 90,000 cycles, the period of the meso-II surface undulations increases up to 1.5 mm, covering about 150 grains. The whole set of surface out-of-plane displacements of different widths and heights, formed by individual grains and grain groups, are seen in the entire surface profiles (black plots in Fig. 3).

In order to estimate how the contributions from different scales were changed in the course of LCF loading, the raw profiles were decomposed into the macro, meso-I and meso-II components which were statistically analyzed in terms of standard deviations. Corresponding data are plotted in Figure 4a as a bar graph. The standard deviations indirectly correspond to the range of the peak-to-valley distance variations. Figure 4a shows that the larger the scale of consideration, the higher the standard deviation value. For all profile components, the standard deviations tend to increase with the number of cycles, intensifying the surface roughness at the meso-I, meso-II, and macro scales (Fig. 4a). The maximum peak-to-valley distance of the entire surface profiles grows progressively with the number of cycles, reaching ~7 µm at the pre-fracture stage (the black curve in Fig. 3b).

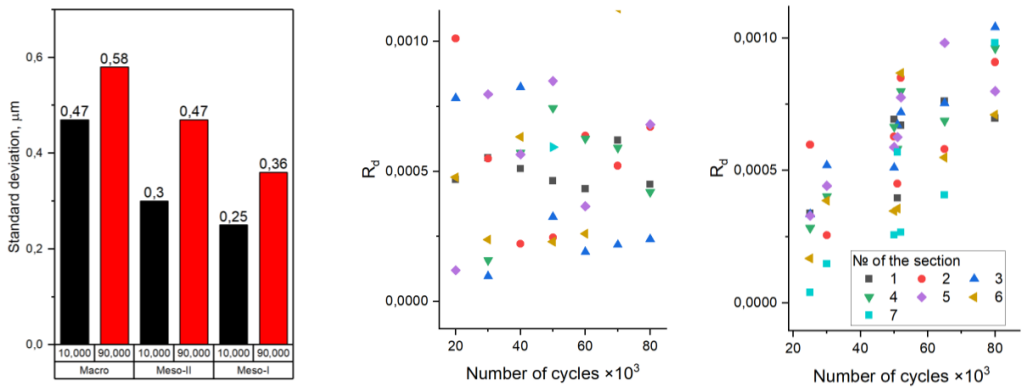

FIGURE 4. Standard deviations of the meso-I, meso-II, and macroscopic surface profile components (a), dependences of the Rd parameter on the number of cycles for the 1st (b) and 2nd (c) test series

In contrast to findings for uniaxial tension [15, 16], the evolution of DISR under LCF develops uniformly across the specimen surface (cf. Fig. 5b and c). In the first series of LCF tests with the constant stress amplitude, the Rd values in the specimen sections change in a saw-tooth manner, demonstrating no persistent increase with the number of cycles (Fig. 4b). This behavior can be attributed to reaching the shakedown limit during the first 10,000 cycles when the material yield strength due to the strain hardening becomes equal to the peak stress of LCF loading [20, 21]. Macroscopically, subsequent deformation under the same stress amplitude remains elastic. The strain fields obtained using DIC confirmed this effect: plastic strain was mostly accumulated during the first 10,000 cycles and ceased to increase in the subsequent LCF loadings (see Fig. 6a and b). Contrastingly, in the second series of LCF tests, where the stress amplitude was gradually increased with the number of cycles, the Rd parameter tended to linearly increase while exhibiting oscillations in individual sections (Fig. 4c).

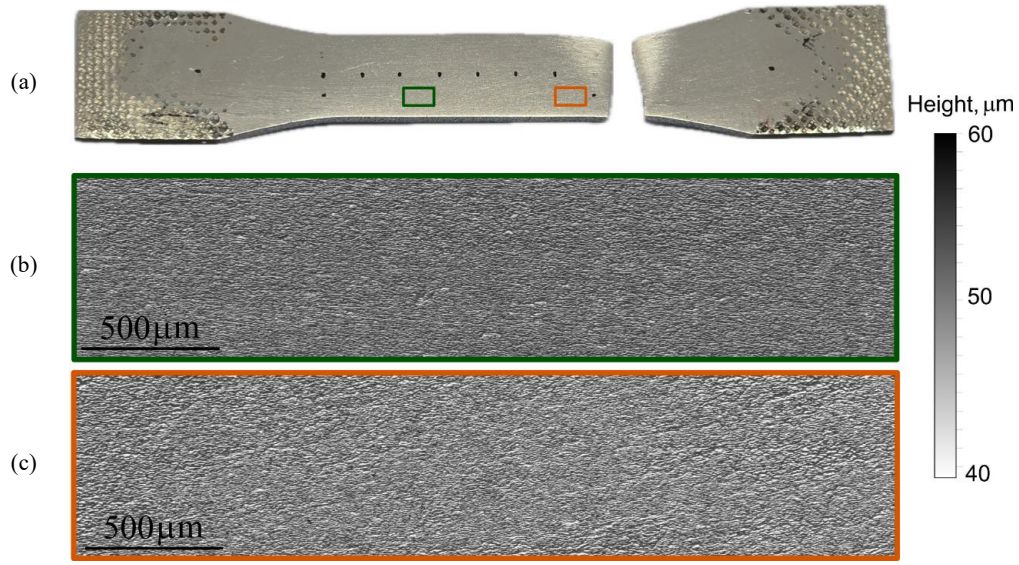

FIGURE 5. Specimen after LCF tests (a) and surface roughness in selected subsections marked by green (b) and red rectangles (c) obtained by optical profiler NewView 6200

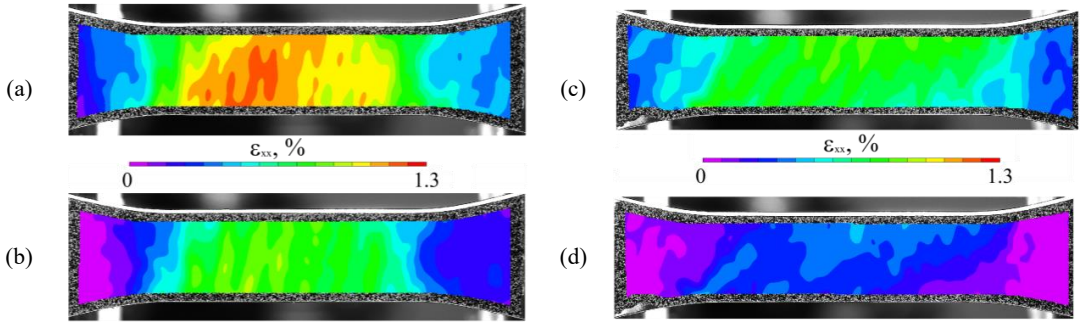

FIGURE 6. DIC snapshots of ε_{xx} strain fields in a CP-Ti specimen after 10,000 (a, b) and 80,000 cycles (c, d) for the peak (a, c) and zero (b, d) stress states in a cycle

CONCLUSION

The multiscale features of deformation-induced surface roughening in CP-Ti specimens under low cycle fatigue loading have been investigated experimentally. It was shown that surface roughening developed uniformly across the specimen gauge parts. The surface morphology comprised a set of multiscale asperities attributed to collective out-of-plane displacements of smaller and larger grain groups. They appeared during the first 10,000 cycles and progressively evolved in the course of LCF loading. The dimensionless roughness parameter did not correlate with the number of cycles under the constant stress amplitude and grew linearly when the LCF peak stress was increased.

ACKNOWLEDGMENTS

This work is supported by Russian Science Foundation through the grant № 24-79-00047 (https://rscf.ru/en/project/24-79-00047/).

REFERENCES

1. M.D. Sangid, The physics of fatigue crack initiation. Int. J. Fatigue **57**, 58–72 (2013). https://doi.org/10.1016/j.ijfatigue.2012.10.009
2. A. A. Shanyavskiy, A. P. Soldatenkov, A. D. Nikitin, Hierarchy of the metal fatigue mechanisms based on the physical mesomechanics methodology. Phys. Mesomech. **6** (2025). https://doi.org/10.1134/S1029959925600120
3. A. A. Shanyavskiy, A. P. Soldatenkov, Relation between stresses for the boundaries of scale levels of the fatigue diagram and difference of the meso- and macroscale fracture mechanisms. Phys. Mesomech. **27**, 256-268 (2024). https://doi.org/10.1134/S1029959924030032
4. V. E. Panin, T. F. Elsukova, Yu. F. Popkova, Stages of multiscale fatigue cracking as a nonlinear rotational autowave process. Phys. Mesomech. **14** (3-4), 112-123 (2011). https://doi.org/10.1016/j.physme.2011.08.003
5. M. Wang, Y. Wang, A. Huang, L. Gao, Y. Li, Ch. Huang, Promising tensile and fatigue properties of commercially pure titanium processed by rotary swaging and annealing treatment. Materials **11** (11), 2261 (2018). https://doi.org/10.3390/ma11112261
6. P. Wang, Z. Xu, P. Zhang, B. Wan, X. Liu, Y. Zhu, R. Liu, Y. Liu, Y. Luan, P. Wang, D. Li, R. O. Ritchie, Zh. Zhang, The highest fatigue strength for steels. Acta Mater. **289**, 120888 (2025). https://doi.org/10.1016/j.actamat.2025.120888
7. H. Li and M. Fu, "Inhomogeneous Deformation-Induced Surface Roughening Defects" in *Deformation based processing of materials: behavior, performance, modeling and control* (Elsevier, Amsterdam, 2019), pp. 225-256.
8. D. Raabe, M. Sachtleber, H. Weiland, G. Scheele, Z. Zhao, Grain-scale micromechanics of polycrystal surfaces during plastic straining. Acta Mater. **51**, 1539-1560 (2003). https://doi.org/10.1016/S1359-6454(02)00557-8

9. E.S. Emelianova, O.S. Zinovieva, V.A. Romanova, R.R. Balokhonov, M. Pisarev, Experimental and numerical investigation of mesoscale deformation-induced surface roughening in polycrystalline metals and alloys (review). Phys. Mesomech. **27** (1), 16-33 (2024). https://doi.org/10.1134/S1029959924010028
10. V. L. Popov, Coefficients of restitution in normal adhesive impact between smooth and rough elastic bodies. Rep. Mech. Eng. **1**, 103–109 (2020). https://doi.org/10.31181/rme200101103p
11. V. L. Popov, Designing surface profiles with zero and finite adhesion. Spec. Mech. Eng. Oper. Res. **1** (1), 82-89 (2024). https://doi.org/10.31181/smeor1120246
12. J. Wilhayan, I. A. Lyashenko, Q. Li, V. L. Popov, Influence of tangential sliding on the contact area of a macroscopic adhesive contact. Facta Univ., Ser. Mech. Eng. **22** (3), 385-397 (2024). https://doi.org/10.22190/FUME240414028W
13. A. A. Burkov, S. V. Nikolenko, V. O. Krutikova, N. A. Shelmenok, Electrospark deposition of Ti-Ta coatings on Ti6Al4V titanium alloy: oxidation resistance and wear properties. Phys. Mesomech. **27**, 618-626 (2024). https://doi.org/10.1134/S1029959924050096
14. N. Daghbouj, H.S. Sen, M. Callisti, M. Vronka, M. Karlik, J. Duchoň, J. Čech, V. Havránek, T. Polcar, Revealing nanoscale strain mechanisms in ion-irradiated multilayers. Acta Mater. **229**, 117807 (2022). https://doi.org/10.1016/j.actamat.2022.117807
15. V. Romanova, E. Emelianova, M. Pisarev, O. Zinovieva, R. Balokhonov, Quantification of mesoscale deformation-induced surface roughness in α-titanium. Metals **13**, 440 (2023). https://doi.org/10.3390/met13020440
16. V. Romanova, R. Balokhonov, E. Emelianova, E. Sinyakova, M. Kazachenok, Early prediction of macroscale plastic strain localization in titanium from observation of mesoscale surface roughening. Int. J. Mech. Sci. **161–162**, 105047 (2019). https://doi.org/10.1016/j.ijmecsci.2019.105047
17. E. Emelianova, M. Pisarev, V. Romanova, Grain-scale plastic strain accumulation in commercially pure Ti under cyclic loading. AIP Conf. Proc. **3177**, 060003 (2025). https://doi.org/10.1063/5.0294822
18. ASTM E466-15 (ASTM International, 2015).
19. V.E. Panin, Overview on mesomechanics of plastic deformation and fracture of solids. Theor. Appl. Fract. Mech. **30**, 1–11 (1998). https://doi.org/10.1016/S0167-8442(98)00038-X
20. G. Chen, Sh. Xin, L. Zhang, M. Chen, C. Gebhardt, Shakedown-reliability based fatigue strength prediction of parts fabricated by directed energy deposition considering the microstructural inhomogeneities. Eur. J. Mech. A-Solid. **103**, 105170 (2024). https://doi.org/10.1016/j.euromechsol.2023.105170
21. V. K. Dang, I. V. Paradopoulos, High-Cycle Metal Fatigue: From Theory to Applications (Springer Wien, Vienna, 1999), 209 p.